Surface fractals in liposome aggregation

Sándalo Roldán-Vargas,[1] Ramon Barnadas-Rodríguez,[2,3] Manuel Quesada-Pérez,[4]
Joan Estelrich,[2] and José Callejas-Fernández[1,*]

[1]*Grupo de Física de Fluidos y Biocoloides, Departamento de Física Aplicada, Universidad de Granada, E-18071 Granada, Spain*
[2]*Departament de Fisicoquímica, Facultat de Farmàcia, Universitat de Barcelona, E-08028 Barcelona, Catalonia, Spain*
[3]*Centre d'Estudis en Biofísica, Facultat de Medicina, Universitat Autònoma de Barcelona, E-08193 Cerdanyola del Vallès Bellaterra, Barcelona, Catalonia, Spain*
[4]*Departamento de Física, Escuela Politécnica Superior de Linares, Universidad de Jaén, Linares, E-23700 Jaén, Spain*

(Received 1 August 2008; published 12 January 2009)

In this work, the aggregation of charged liposomes induced by magnesium is investigated. Static and dynamic light scattering, Fourier-transform infrared spectroscopy, and cryotransmission electron microscopy are used as experimental techniques. In particular, multiple intracluster scattering is reduced to a negligible amount using a cross-correlation light scattering scheme. The analysis of the cluster structure, probed by means of static light scattering, reveals an evolution from surface fractals to mass fractals with increasing magnesium concentration. Cryotransmission electron microscopy micrographs of the aggregates are consistent with this interpretation. In addition, a comparative analysis of these results with those previously reported in the presence of calcium suggests that the different hydration energy between lipid vesicles when these divalent cations are present plays a fundamental role in the cluster morphology. This suggestion is also supported by infrared spectroscopy data. The kinetics of the aggregation processes is also analyzed through the time evolution of the mean diffusion coefficient of the aggregates.

DOI: 10.1103/PhysRevE.79.011905 PACS number(s): 87.16.dr, 87.64.Cc, 82.70.−y

I. INTRODUCTION

Aggregation of mesoscopic biological objects such as micelles, vesicles, and large macromolecules has generally a great relevance. In physics, it could shed light on the relationship between the structure and kinetics of the aggregates and the relative strength of diverse interaction forces (electrostatic, magnetic, steric, depletion, etc.). In biology, knowledge of the interaction mechanism at short distances between these objects immersed in an electrolyte solution is a key to elucidation of essential biological processes involved in many cellular phenomena, e.g., membrane fusion [1,2]. Here, we focus on the morphological and kinetic aspects of the aggregates formed by liposomes made of phosphatidilserine (PS), which is the major anionic phospholipid of many cell membranes.

Fractal geometry can be used to describe the morphology of the clusters through the measurement of their fractal dimension [3]. In this framework, many of the morphologies formed in aggregating colloidal systems have been identified as *mass fractals*: Their mass M scales with their radius R as $M \propto R^{d_m}$ ($d_m \leqslant 3$), d_m being the *mass fractal dimension*. In this way, more or less branched clusters ($1.75 \leqslant d_m \leqslant 2.1$) have been reported in irreversible aggregation [4] whereas dense cluster structures have been documented, even with $d_m > 2.5$, when internal restructuring is allowed [5,6]. In particular, it is a commonplace to speak of *dense* morphologies when d_m is larger than 2.5. In that case, the underlying physics of these high d_m values has rarely been explored. Moreover, we suspect that some of these large d_m values could be attributed to a wrong interpretation of the experimental data, due to the nonconsidered effect of the multiple scattering on the experimental determination of the fractal dimensions of dense objects.

In addition to mass fractals, another class of dilation symmetry has been described for uniform structures ($d_m = 3$) limited by a fractal rough surface S which scales with the radius of the object as $S \propto R^{d_s}$ ($2 \leqslant d_s < 3$) [7]. These objects are known as *surface fractals* and d_s is their *surface fractal dimension*. In the literature, and from an experimental viewpoint, it is difficult to find aggregation phenomena (or others related to them) described using the concept of the surface fractal. A noticeable exception is the work of Keefer and Shaefer [8] on the growth of silicate particles in solution.

In a recent study on PS liposome aggregation induced by calcium, a transition from $d_m = 1.91$ to 1.75 for the mass fractal dimension of the resulting structures was observed, by means of static light scattering (SLS), when the calcium concentration increased from 2.5 to 5 mM. Convergence to a diffusion-limited cluster aggregation (DLCA) regime, $d_m = 1.75$, was also experimentally documented [9]. More recently, we have described in a short communication a transition from surface fractal to mass fractal structures in a suspension of aggregating liposomes, using the divalent cation Mg^{2+} as aggregating agent [10]. This change in the morphology of the clusters is controlled by the amount of magnesium added and shows a final stable value of the mass fractal dimension appreciably larger, $d_m = 2.6-2.7$, than that corresponding to the DLCA regime previously documented in our calcium study.

In this paper, a considerably detailed description and analysis of both structural and kinetic aspects of this surface to mass fractal transition controlled by the magnesium concentration are presented. The interaction energies involved in these aggregation processes are also discussed in the light of the experimental data. In this way, the previous report [10] is

*jcalleja@ugr.es

well completed. From the experimental point of view, the influence of the multiple intracluster scattering (MIS) and polydispersity of the aggregates on the measured fractal dimensions are widely discussed. The morphologies revealed by our SLS study are also supported by cryotransmission electron microscopy (cryo-TEM) micrographs. At the same time, our analysis of the aggregation phenomenon is completed with a study of the aggregation kinetics. To do that, the experimental time evolution of the mean cluster diffusion coefficient is measured by means of dynamic light scattering (DLS) and compared with the theoretical result obtained from the resolution of Smoluchowski's equation.

Discussing the influence of the total interaction energy between liposomes on the resulting cluster morphologies, we will also argue that the classical Derjaguin-Landau-Verwey-Overbeek (DLVO) theory (which considers only the Coulomb and van der Waals interactions [11,12]) is not suitable in this case. In this respect, it is well known in biophysics that the phospholipid head groups belonging to the surface of the lipid vesicles are more or less hydrated. Thus, a hydration energy may appear. In fact, some authors claim [13–15] that this hydration interaction energy could play a key role in the liposome aggregation. Hence, we decided to analyze the dehydration effect due to magnesium and calcium ions from Fourier-transform infrared spectroscopy (FTIR). This analysis suggests that the hydration grade of the lipid molecule in the presence of these two divalent cations plays an essential role in the vesicle short-range interaction mechanism and conditions the resulting cluster morphology.

The rest of the paper is organized as follows. First, the theoretical background is outlined. Section III contains a detailed description of the experimental procedures and methods. Then, the main results of the work and the corresponding discussion are presented and, finally, some conclusions of this research are highlighted.

II. BACKGROUND

A. Surface and mass fractals: Concept and measurement

In a pioneering work, Pfeifer and Avnir proposed the application of fractal theory to characterize heterogeneous chemical surfaces [7]. In that investigation, surfaces with different degrees of irregularity (roughness) were labeled by a real number d, where $2 \leqslant d < 3$, if certain conditions were satisfied.

Let us specify these conditions by considering the usual ball-covering process of a rough surface in three-dimensional space, i.e., the covering of the whole surface with the minimal number $N(r)$ of balls of radius r providing that any point of the surface is included in at least one of the balls. It is clear that with decreasing r the number $N(r)$ grows generally in a nontrivial fashion. If the covering process satisfies the existence of the limit

$$\lim_{r \to 0} \frac{\ln N(r)}{\ln r} = d \quad (d \in [2,3[), \tag{1}$$

the surface will be called a *fractal surface* and its roughness, which is persistent at different spatial scales, will be described by d, the *surface fractal dimension*. If the fractal surface under consideration is closed and it defines the boundary of a completely compact three-dimensional object (a "walnut" [16]), this object will be called a *surface fractal*, having a surface fractal dimension d. Therefore, from these definitions, the distinction between a fractal surface and a surface fractal is evident (for more details see Ref. [17]).

If we associate a characteristic length with our *surface fractal*, e.g., its radius of gyration R, an equivalent expression for (1) can be found if we dilate the object by a growth factor, keeping constant the radius r of the covering balls. Then, asymptotically $(R \to \infty)$,

$$S = KR^d \quad (2 \leqslant d < 3), \tag{2}$$

where S is the covering surface of the surface fractal and K is a positive real number. Accordingly, from $d=2$ (smooth surface) the roughness of a surface fractal increases with increasing d.

Certainly, as is well known, the process described above can be extended to the covering of the volume of a three-dimensional object which in general will not be completely compact. If we now start the covering process in an inner point of the object and continue our covering from this point by increasing the distance R, remaining always inside the object, we shall called this object a *volume* or *mass fractal* if the covering volume V scales as

$$V \propto R^d \quad (d \leqslant 3). \tag{3}$$

Similarly, d, now called the *mass fractal dimension*, is an estimation of the compactness (not the roughness) of the mass fractal: from $d=3$ (uniform object), the compactness of a mass fractal decreases with decreasing d.

Nevertheless, it must remain clear that two different surface fractals show different fractal properties only on their boundaries whereas their interiors are uniform. Then, for clarity, we shall identify by $d_s=d$ the fractal dimension corresponding to definition (2) and by $d_m=d$ when it corresponds to (3). With this notation, a surface fractal will always be described by $2 \leqslant d_s < 3$ and $d_m=3$.

In order to probe the emergence of fractal structures in colloidal aggregation such as those described by (2) or (3), a widely used technique is static scattering in its different versions (x rays, neutrons, or light). In this sort of measurement an experimental value of the structure factor $S(q)$ of the analyzed sample is accessible [18]:

$$S(q) = \frac{1}{N} \sum_{i=1}^{N} \sum_{j=1}^{N} \langle e^{i\vec{q}\cdot(\vec{r}_i - \vec{r}_j)} \rangle_{\text{ensemble}}, \tag{4}$$

where $\vec{q}$ is the scattering vector, $\vec{r}_i$ and $\vec{r}_j$ represents the positions of the ith and jth scatterers, N is the number of particles (scatterers), and $\langle \cdots \rangle_{\text{ensemble}}$ represents the ensemble-averaged value. Thus, the term $\vec{q} \cdot (\vec{r}_i - \vec{r}_j)$ indicates whether the scattering waves combine constructively or randomly at the detector. Then, $S(q)$ reveals, through its q dependence, the structure of the system. Here, we focus on the light scattered by a system of aggregates constituted of colloidal particles.

From a general point of view, the fractal nature of a structure within a given spatial scale is proved by a power law dependence of $S(q)$ within a given q range. Thus, if a structure presents a fractal nature between two characteristic lengths, a power law dependence of $S(q)$ is expected when q^{-1} is included between these characteristic lengths. In this respect, and in order to test the fractal nature of rough surfaces, Bale and Schmidt [19] were the first to propose a functional behavior for $S(q)$, applying their model to the study of lignite coal. On the other hand, starting from the work of Schaefer and co-workers [20], several experimental studies have been performed in order to prove the structure of mass fractals. A compendium of their results is

$$S(q) \propto q^{-\alpha}, \tag{5}$$

where $\alpha=d_m$ (mass fractals) and $\alpha=2d_m-d_s=6-d_s$ (surface fractals). In the case that the fractal structures are aggregates of representative radius R made of subunits of characteristic radius a, expression (5) will be typically satisfied within $R^{-1} \ll q \ll a^{-1}$.

From a physical point of view, the scattering phenomenon comes from the fluctuations in the density of the scatterers. In a mass fractal, essentially all the primary particles are on the surface, there are no inner particles, and the density fluctuations come from any point of the structure. In a surface fractal, only a fraction of the primary particles belong to the surface; the rest are inner particles. In this kind of fractal, internal fluctuations do not contribute significantly to the scattered intensity [21].

B. Structure factors in aggregated systems: Effect of the multiple scattering

In a lighted colloidal dispersion, a fraction of the incident photons is scattered twice or more in passing through the sample; this is known as multiple scattering. This phenomenon is always present even though the initial nonaggregated suspension is diluted, having a small concentration of "scatterer material," i.e., when the first Born approximation is satisfied [4,22]. In aggregation, however, the light scattered by an aggregate is rarely scattered again by others if the suspension is sufficiently diluted. In contrast, multiple reflections inside the aggregates do take place. This is called multiple intracluster scattering (MIS). To clarify the incidence of this MIS on the determination of fractal dimensions, great efforts have been made from the theoretical and experimental points of view, at least for mass fractals; see, for instance, [21,23,24]. In this respect, experimental designs based on cross-correlation schemes [25–27] have proved to be successful in reducing to a negligible amount the multiple scattering in stabilized dense colloidal suspensions. Here we provide a basic theoretical description of one of these schemes, three-dimensional dynamic light scattering (3D-DLS) [26], which will be applied to an aggregating system. This description has been essentially adapted from [28].

Accordingly, two laser beams with equal wavelength and intensities coming from above and below an average scattering plane are focused onto a colloidal dispersion. At the same time, a digital correlator computes the cross-correlation function of the scattered intensities registered by two detectors (1 and 2) which are positioned at an equal scattering angle (i.e., they are positioned at an equal q value). For a dilute nonaggregated system, the time-averaged singly scattered intensity $\langle I^0_{1,2}(q)\rangle^{\text{volume}}_{\text{single}}$ coming from the scattering volume is

$$\langle I^0_{1,2}(q)\rangle^{\text{volume}}_{\text{single}} = A_{1,2}\phi P(q), \tag{6}$$

where $A_{1,2}$ includes the incident laser intensities and other constants of proportionality, whereas ϕ and $P(q)$ are the particle volume fraction and the form factor of the primary particles, respectively. Similarly, for a dilute aggregated system, the corresponding time-averaged singly scattered intensity coming from the scattering volume, denoted now by $\langle I^a_{1,2}(q)\rangle^{\text{volume}}_{\text{single}}$, is given by

$$\langle I^a_{1,2}(q)\rangle^{\text{volume}}_{\text{single}} = A_{1,2}\phi P(q)S(q), \tag{7}$$

where $S(q)$ is the structure factor of the aggregated system. By virtue of the statistical properties of the scattered signal, $\langle I^{\text{system}}_{1,2}(q)\rangle^{\text{volume}}_{\text{single}}$ (system $\in\{a,0\}$) can be factorized as a product of the registered signals: $\langle I^{\text{system}}_{1,2}(q)\rangle^{\text{volume}}_{\text{single}} = \sqrt{\langle I^{\text{system}}_{1}(q)\rangle^{\text{volume}}_{\text{single}}\langle I^{\text{system}}_{2}(q)\rangle^{\text{volume}}_{\text{single}}}$, $\langle I^{\text{system}}_{i}(q)\rangle^{\text{volume}}_{\text{single}}$ being the time-averaged singly scattered intensity coming from the scattering volume and registered at detector i ($i=1$ or 2). Then we obtain $S(q)$ from expressions (6) and (7):

$$S(q) = \sqrt{\frac{\langle I^a_1(q)\rangle^{\text{volume}}_{\text{single}}\langle I^a_2(q)\rangle^{\text{volume}}_{\text{single}}}{\langle I^0_1(q)\rangle^{\text{volume}}_{\text{single}}\langle I^0_2(q)\rangle^{\text{volume}}_{\text{single}}}}. \tag{8}$$

Note that ϕ was removed because the initial and the aggregated samples have identical particle volume fractions.

However, on propagating from the scattering volume to the wall of the scattering cell, the scattered signals suffer attenuation and only a fraction of the scattered photons will reach the detectors. This fraction is accounted for by the system's transmission coefficient $T^{\text{system}}_i = \langle I^{\text{system}}_i(q)\rangle^{\text{out}}_{\text{single}}/\langle I^{\text{system}}_i(q)\rangle^{\text{volume}}_{\text{single}}$, where $\langle I^{\text{system}}_i(q)\rangle^{\text{out}}_{\text{single}}$ is the time-averaged singly scattered intensity that would reach detector i after the attenuation effect. At the same time, although the structure and form of the primary particles are related through expressions (6) and (7) to the singly scattered intensities, in practice we detect a mixture of intensities (single+multiple). Although we do not have direct access to the singly scattered intensities, a cross-correlation scheme like 3D DLS allows us to obtain the ratio between the required single-scattering intensities and the total measured intensities as will be discussed in Sec. III C. This ratio is represented by $[\beta^{\text{system}}(q)]^2$:

$$[\beta^{\text{system}}(q)]^2 = \frac{\langle I^{\text{system}}_1(q)\rangle^{\text{out}}_{\text{single}}\langle I^{\text{system}}_2(q)\rangle^{\text{out}}_{\text{single}}}{\langle I^{\text{system}}_1(q)\rangle\langle I^{\text{system}}_2(q)\rangle}, \tag{9}$$

where $\langle I^{\text{system}}_i(q,t)\rangle$ is the total (single+multiple scattering) time-averaged intensity registered at detector i for a given system. Therefore $\beta^{\text{system}}(q)$ computes the contribution of the multiple scattering. It is clear that for a dilute system $\beta(q)\approx 1$. Substitution of Eq. (9) and $T^{\text{system}}_i = \langle I^{\text{system}}_i(q)\rangle^{\text{out}}_{\text{single}}/\langle I^{\text{system}}_i(q)\rangle^{\text{volume}}_{\text{single}}$ in Eq. (8) finally gives

$$S(q) = \sqrt{\frac{\langle I_1^a(q)\rangle\langle I_2^a(q)\rangle}{\langle I_1^0(q)\rangle\langle I_2^0(q)\rangle}}\sqrt{\frac{T_1^0 T_2^0}{T_1^a T_2^a}\frac{\beta^a(q)}{\beta^0(q)}}. \quad (10)$$

Thus $S(q)$ is expressed in terms of measurable quantities.

C. Aggregation kinetics

Regarding the aggregation kinetics, it is possible to consider the movement of an aggregate as a solid body by distinguishing a rotational and an isotropic translational diffusion. For the q range and the mean cluster sizes studied in this work (mean hydrodynamic radius greater than 1 μm), the relaxation time associated with the rotational diffusion is at least two orders of magnitude greater than the relaxation time associated with the translational diffusion [29]; thus we assume that these two diffusions are temporally separated. On the other hand, the restructuring movement due to cluster compactification should be considered, at least *a priori*, if the bound between two particles of an aggregate is weak enough. Although this effect has a great influence on the value of the fractal dimension (as we will comment later), we will assume (as other authors do [30]) that restructuring happens during a time of the order of the aggregation process, being conditioned by the cluster size. Therefore, the translational diffusion of an n-particle cluster will be temporally separated from the dynamics of the rest of the system. Thus, the time scale corresponding to our aggregation kinetics study will be associated with the temporal evolution of the translational diffusion coefficient of the clusters with a typical length scale associated with their mean hydrodynamic radius.

In order to obtain the experimental average of the translational diffusion coefficient $\bar{D}_{\text{expt}}(q;t)$ over the system at any time, the *normalized electric field autocorrelation function* $g_E(\tau)=\langle E(q,0)E^*(q,\tau)\rangle/\langle|E(q)|^2\rangle$ is treated as an expansion in powers of τ [31]:

$$\ln[g_E(\tau)] = -\kappa_1\tau + \frac{1}{2}\kappa_2\tau^2 + \cdots, \quad (11)$$

where κ_i is the ith-order cumulant. Thus, κ_1 gives the average decay rate whereas κ_2 contains the standard deviation. In this context,

$$\bar{D}_{\text{expt}}(q;t) = \kappa_1/q^2. \quad (12)$$

From a theoretical viewpoint, an estimation of the mean translational diffusion coefficient $\bar{D}(q;t)$ can be performed at any time by means of an average of the diffusion coefficients D_n of the n-particle clusters:

$$\bar{D}(q;t) = \frac{\sum_{n=1}^{N_c} b_n(q;t)D_n}{\sum_{n=1}^{N_c} b_n(q;t)}, \quad (13)$$

where $b_n(q;t)=N_n(t)n^2S(qR)$ contains the frequency and the structure of the n-particle clusters [32], $N_n(t)$ is the frequency of the n-particle clusters at time t, and $S(qR)$ is their corresponding structure factor, R being again the radius of gyration of the n-particle cluster. At long times, i.e., when the aggregates reach a nonevolving fractal morphology, an estimation of D_n can be made by assuming that the cluster compactness is given by the final mass fractal dimension d_m:

$$\frac{D_n}{D_0} = (n)^{-1/d_m} \propto R^{-1}, \quad (14)$$

where D_0 is the diffusion coefficient of the free individual particles.

The assumption of a functional form for $S(qR)$ within all accessible values of qR involves a problem with an unknown analytical solution that has only been estimated by means of computer simulations [32]. However, this difficulty can be overcome if our estimation of $\bar{D}(q;t)$ is performed for $qR \gg 1$. In that case, the fractal structure is resolved and $S(qR) \propto (qR)^{-d} \propto n^{-1}q^{-d}$. Therefore, only an *a priori* knowledge of $N_n(t)$ is needed in order to obtain the theoretical mean translational diffusion coefficient given by Eqs. (13) and (14).

The frequency $N_n(t)$ can be predicted if the aggregating suspension is diluted enough (monomer volume fraction usually below 1%). In this respect, the aggregation process can be considered as a set of binary reactions $A_i+A_j \rightarrow A_{i+j}$ (A_i denotes an aggregate formed by i monomers) neglecting the simultaneous reactions involving three or more clusters [33]. A widely used mean-field aggregation model based on the binary reaction assumption is Smoluchowski's rate equation [34,35]. Its expression for reactions in which fragmentation does not take place is

$$\frac{dN_n(t)}{dt} = \frac{1}{2}\sum_{i+j=n} k_{ij}N_i(t)N_j(t) - N_n(t)\sum_{i=1}^{\infty} k_{in}N_i(t). \quad (15)$$

The set of rates k_{ij} ($i,j=1,\ldots,\infty$), usually known as the *kernel*, contains the whole kinetic information through its mass (number of monomers) and geometry cluster dependences. From a known k_{ij} and an initial condition, e.g., $\vec{N}(0)=(N_1(0)=1,N_2(0)=0,\ldots,0)$, expression (15) gives a continuous and deterministic set of frequencies $\vec{N}(t)$ at any time.

Due to the difficulty of assuming a functional form for the reaction kernel, it is useful to consider its asymptotic behavior under the homogeneous scheme of van Dongen and Ernst [36]. In this context, small-large and large-large cluster interactions are governed by two exponents ν and λ: $k_{1j} \propto j^{\nu}$ and $k_{jj} \propto j^{\lambda}$ (large j). This scaling theory applied to nongelling kernels ($\lambda \leqslant 1$) also provides the asymptotic behavior of $\bar{D}(q;t)$:

$$\bar{D}(q;t) \propto t^{-z}, \quad [z = 1/(1-\lambda)d_m]. \quad (16)$$

In fact, expression (16) is a key to associating a type of kernel to the results obtained from the experimental kinetics of an aggregation process.

Pure diffusion aggregation processes have also a special interest under this formalism. On one hand, these processes are dominated by small-large cluster interactions whereas interactions between identical-sized clusters do not show any dependence on j for large j ($k_{jj} \propto j^{\lambda=0} \approx \text{const}$) due to the compensation between the increasing collision cross section

and the decreasing diffusivity of the clusters when j grows [37].

D. Interactions between liposomes

From a physicist's viewpoint, charged liposomes can be considered as colloidal particles whose interactions can be treated with the help of a well-known mean-field approach: The DLVO theory. Accordingly, the lipid vesicles would interact through Coulomb repulsive forces (characterized by an interaction energy E_{elec}) and short-range van der Waals attractive forces (whose interaction energy will be denoted by E_{vW}). Usually, E_{elec} is modeled as a Yukawa decaying function that contains as input parameters the Debye length and the surface potential (or charge). For E_{vW}, Hamakers constants of water, hydrocarbon, and the polar phase, together with the thickness of the surface phospholipid layer, have been used as input parameters.

Apart from classical DLVO theory, when colloidal particles have a surface with a certain degree of hydrophobicity, different experimental techniques and theoretical approximations [13–15] have pointed out the existence of a hydration energy E_{hyd}, which is generally repulsive. In the 1970s, the origin of this hydration or structural force was mainly attributed to the strongly bound and oriented layers of water molecules on the surfaces [13]. However, there are other possible explanations such as the local variation of the dielectric permittivity in the electric double layer [14] or an entropic repulsion arising from the confinement of thermally mobile surface groups [15]. Thus, a conclusive comprehension of E_{hyd} is still lacking and to find an analytical expression for E_{hyd} is not a straightforward task. For that reason, experiments and computer simulations based on statistical mechanics incorporating even quantum effects should be used in coming years. In their absence, some authors use semiempirical exponential expressions for E_{hyd} that also introduce fitting parameters [38,39] in order to explain experimental results. In particular, Okhi and Arnold define a hydrophobic index that represents the degree of hydrophobicity of the membrane surface [39]. They propose to model the hydration energy from a purely repulsive interaction (the surface is hydrophilic and tends to be completely hydrated) to an attractive interaction (the surface is hydrophobic and then it is largely dehydrated). In this model, the surface tension of the present interfaces also appears as an input parameter, together with the hydrophobic index.

In our work, the importance of E_{hyd} in the aggregation processes mediated by divalent cations will be experimentally analyzed via FTIR spectroscopy. Thus, we will conclusively show that the dehydration of the superficial lipid head groups exerted by some metallic cations must be considered. Due to the large number of parameters involved in the total interaction energy, $E=E_{elec}+E_{vW}+E_{hyd}$, a qualitative (rather than quantitative) analysis will be preferred in order to explain our experimental results.

III. MATERIALS AND METHODS

A. Synthesis and characterization of liposomes

Phosphatidilserine from bovine spinal cord was obtained from Lipid Products (Nutfield, U.K.). Phospholipids at the proportions indicated below were dissolved in a mixture (2:1, volume ratio) of chloroform and methanol in a round-bottom flask and dried in a rotary evaporator under reduced pressure at 40 °C to form a thin film on the flask. The film was hydrated with deionized water (MilliQ, Millipore, U.S.A.) to give a lipid concentration of 30 mM. Multilamellar liposomes (MLVs) were formed by constant vortexing for 4 min on a vortex mixer and sonication in a Transonic Digitals bath sonifier (Elma, Germany) for 10 min. MLVs were downsized in an Extruder device (Lipex Biomembranes, Canada) through polycarbonate membrane filters of variable pore size under nitrogen pressures of up to 55×10^5 N m^{-2}. Liposomes were extruded in three steps. First, three consecutive extrusions were performed through a 0.8 μm pore diameter filter and then three consecutive extrusions through two stacked 0.4 μm membranes. The resulting lipid suspension was then extruded 15 consecutive times through two stacked 0.2 μm filters. After preparation, a nitrogen stream was passed to displace the air, and, finally, liposomes were stored at 4–7 °C in a refrigerator in quiescent conditions until their use.

To characterize a liposome suspension as a colloidal dispersion, two different requirements are necessary: the characterization of particles in size and shape and the determination of the initial liposome concentration, which is a troublesome problem when vesicles are used as primary particles. In order to determine the liposome size, DLS and SLS experiments were performed for different dilute liposome volume fractions and angles. In the case of DLS, the size was obtained from the mean particle diffusion coefficient, $\bar{D}_{expt}(q;t)$, which was in turn determined using the cumulant analysis [expression (12)], by averaging six individual measures at different scattering angles. By means of SLS, the particle size was determined by fitting the particle form factor of a three-modal distribution of hollow spheres, since the liposomes were assumed to be unilamellar vesicles within certain degree of polydispersity (see Ref. [9] for a more detailed explanation). The best agreement was reached for a mean radius $a=75$ nm and polydispersity of 0.2 (standard deviation of the particle radius divided by the mean). This size and a thickness of 4.5 nm, obtained by means of small angle x-ray scattering, typify our liposomes as *large unilamellar vesicles*.

To measure the initial liposome concentration, the procedure proposed by Haro-Perez *et al.* [40] has been followed. This method compares the volume fraction obtained by assuming that the whole PS mass is forming vesicles with that obtained considering a homogeneous distribution of repulsively structured vesicles. The values obtained differ by about 3.5%.

B. Aggregation experiments

Aggregation was induced by adding electrolyte to the initially stable aqueous suspensions of liposomes at 25 °C. The water used for sample preparation was purified by inverse osmosis using Millipore equipment. The different electrolyte-particle mixtures were prepared by mixing equal amounts of buffered electrolyte solution and particle suspen-

sion in a Y-shaped mixing device in a cylindrical quartz glass cuvette. The magnesium concentration was varied from 5 to 150 mM of $MgCl_2$. In all cases, the final liposome volume fraction was 0.1%. The experimental threshold salt concentration to induce aggregation was $[MgCl_2]=4$ mM. No change in time of the first cumulant of the field autocorrelation function was observed for smaller salt concentrations, which confirms the existence of such a threshold.

C. Experimental measurement of the structure factor and the diffusion coefficient

On the basis of the 3D DLS scheme discussed in Sec. II B, our light scattering experiments were performed with the help of a 3D DLS spectrometer equipped with a rotatory arm, supplied by LS instruments (Fribourg, Switzerland). Formally, in this design the scattering volume is defined by the intersection between the collecting optics and the cross of two incident incoherent He-Ne laser beams (wavelength *in vacuo* $\lambda=632.8$ nm) coming from above and below the average scattering plane. A digital correlator computes the *normalized cross-correlation function* $g_{12}^{\text{system}}(q,\tau)=\langle I_1^{\text{system}}(q,t)I_2^{\text{system}}(q,t+\tau)\rangle/\langle I_1^{\text{system}}(q)\rangle\langle I_2^{\text{system}}(q)\rangle$ of the intensities registered by the two detectors for a given system. These scattered intensities are photomultiplied by two avalanche photodiodes coupled to the arm. The cross-correlation function $g_{12}^{\text{system}}(q,\tau)$ is also recorded by the same computer that controls the spectrometer.

In order to obtain $S(q)$, according to Sec. II B, the function $\beta^a(q)/\beta^0(q)$ that corrects the magnitude of the structure factor due to the disturbance of multiple scattering has to be evaluated [see expression (10)]. Expression (9) is not applicable since we do not have direct access to the singly scattered intensities. In this respect, as was mentioned above, our cross-correlation scheme provides an experimental determination of $g_{12}^{\text{system}}(q,\tau)$. The cross-correlation function is related to the normalized single-scattering dynamic structure factor $g_E(\tau)$ [28] by

$$g_{12}^{\text{system}}(q,\tau)=1+C\beta^{\text{system}}(q)[g_E(\tau)]^2, \tag{17}$$

where $C\leqslant 1$ is a constant that accounts for the different scattering volumes seen by the two detectors and the ratio of the size of the detector apertures to the size of the coherent areas of the scattered light. Expression (17) can be used to determine $\beta^{\text{system}}(q)$ taking advantage of the zero limit $\lim_{\tau\to 0} g_E(\tau)=1$ [28] and then $g_{12}^{\text{system}}(q,\tau=0)=1+C\beta^{\text{system}}(q)$. Thus, if the measurements on the aggregated and nonaggregated systems are performed under identical experimental conditions, C will remain invariant and

$$\left(\frac{\beta^a(q)}{\beta^0(q)}\right)^2=\frac{g_{12}^a(q,\tau=0)-1}{g_{12}^0(q,\tau=0)-1}. \tag{18}$$

By means of expression (18) we make a quantitative measurement of $\beta^a(q)/\beta^0(q)$.

At the same time, we consider as constant factors, within the explored q range, the transmission ratios between the aggregated and nonaggregated samples [expression (10)]. So their influence on the scattering exponents as a multiplicative constant can be discarded [expression (5)]. Therefore, we adopt the experimental determination of an "effective" structure factor $S^*(q)$:

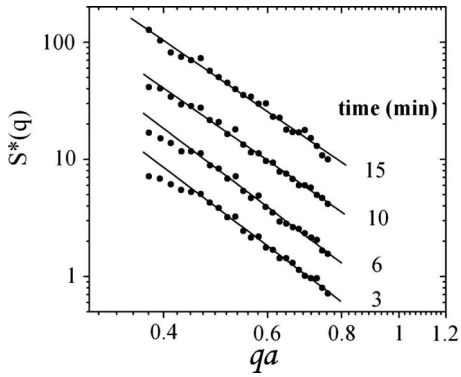

FIG. 1. Experimental $S^*(q)$ according to expression (19) at 5 mM of magnesium. The diverse measurements correspond to different times at which the aggregation process was stopped. Differences in the slope of $S^*(q)$ are negligible after 10 min from the beginning of the aggregation process. From that moment, $S^*(q)$ presents a power law behavior over the entire q range with a nonevolving slope of −3.46 (see also Fig. 5 and Table I). At previous times, $S^*(q)$ presents an evolving behavior; thus the lines corresponding to 3 and 6 min are guides to the eye.

$$S^*(q)=\sqrt{\frac{\langle I_1^a(q,t)\rangle\langle I_2^a(q,t)\rangle}{\langle I_1^0(q,t)\rangle\langle I_2^0(q,t)\rangle}}\frac{\beta^a(q)}{\beta^0(q)}. \tag{19}$$

With the aim of obtaining a reliable determination of $S^*(q)$ for each electrolyte concentration, the aggregation processes were stopped at different times until a constant value for the fitting scattering exponent was reached [expression (5)]. The stops were carried out by diluting the evolving system below the threshold aggregating salt concentration. At their final states, the apparent mean hydrodynamic radius of the aggregates exceeded 1.5 μm for all the samples. Figure 1 shows an example of the time evolution of $S^*(q)$.

Certainly, the q range employed to determine the scattering exponents appears as a crucial point. In this respect, sufficient, but not necessary, conditions have been proposed by different authors in order to obtain reliable values for the scattering exponents; see, for instance, Ref. [41]. Here, in addition to the constraint introduced by the primary particle radius a ($q<a^{-1}$), we have an experimental difficulty due to the rapid increment of the scattered intensity for small q values, which is caused by the large scattering exponents. In this situation, the saturation limit of the detectors is promptly achieved when q decreases and the proportionality between the scattered intensity and the photomultiplied signal becomes broken. This difficulty seems to be present in other SLS measurements involving large scattering exponents; see, for instance, Ref. [42] where the authors found a characteristic scattering exponent of −3.38 using a similar q range to ours.

In order to overcome this problem, we performed our measurements under the saturation limit of the detectors, i.e., in the linear range. Thus, we extended our q range to large q values for which the saturation limit is not achieved. At the

same time, we tested the reliability of the employed q range by reproducing satisfactorily the universal DLCA fractal dimension (d_m=1.75) obtained in our previous study at 5 mM of calcium [9]. This diffusive regime at 5 mM of calcium had been also proved from aggregation kinetics data obtained via independent DLS measurements (see again [9]). At the same time, we confirmed for the explored q range that a reliable and reproducible statistical estimator to determine our structure factors resulted from the average of five independent measurements per q value and 1 min per measurement.

With respect to the system aggregation kinetics, the experimental average value for the translational diffusion coefficient $\bar{D}_{\text{expt}}(q;t)$ at any time was evaluated from expressions (11) and (12). In this case, the scattered field autocorrelation function $g_E(\tau)$ was obtained from the intensity autocorrelation function via the Siegert relation, and was recorded with our computer at intervals of 25 s during the aggregation process. The measures were performed at a fixed angle of 90°.

D. Cryo-TEM measurements

With the aim of complementing our structural study based on light scattering experiments, we took cryo-TEM images from an aggregated sample containing a small concentration of magnesium which is similar to that used in some of our light scattering experiments. At the same time, cryo-TEM measurements were performed for a nonaggregated sample, i.e., in the absence of salt. For the case of the sample containing magnesium, the appropriate volume of a concentrated salt solution was added to the liposome suspension and the suspension was vortexed. After 5 min, a drop of the mixture was deposited on a perforated grid (Quantifoil, Germany), previously ionized by glow discharge in air, and, after part of the drop was removed with a filter paper strip, it was immediately frozen by dipping it in ethane at −182 °C using a Cryo Work Station EM CPC (Leica Microsystems GmbH, Germany). This lag time allows us to obtain liposome aggregates whose size is bigger that 1 μm. This size was previously verified by means of DLS. For the case of samples without salt, a drop of the initial liposome suspension was employed, and the same treatment was done. The obtained grids containing the samples were maintained frozen with liquid nitrogen in a cryo holder and loaded into a transmission electron microscope Jeol JEM-1400 (Jeol Ltd, Tokyo, Japan) working at 120 kV.

E. FTIR measurements

The FTIR spectra of liposomes prepared in D_2O containing the appropriate amounts of the desired cations were acquired with a Mattson Polaris spectrometer. The intensity of the infrared absorption was quantified by means of a cooled liquid nitrogen mercury-cadmium telluride detector. Each spectrum was a mean of 1000 individual scans performed at 25 °C, at a resolution of 2 cm^{-1} and using two CaF_2 windows with a 50 μm spacer containing the sample. The final spectra were obtained by subtracting the spectra of the corresponding solvent acquired in the same conditions. It is known that chemical groups of the phospholipid molecule, like phosphate or carboxylate, can interact with cations, resulting in a change in their vibrational state [43], but the stretching band of the carbonyl ester, located at 1720 cm^{-1}, has been proved to be very sensitive to environmental factors such as, for example, the hydration grade of the molecule [44], the phase state of the bilayers, or the temperature. For these reasons, we focused our attention on the stretching band of the carbonyl ester. This stretching band presents a fine structure composed of minor bands corresponding to the hydrated and nonhydrated carbonyl ester groups. We analyzed the contribution of the nonhydrated carbonyl band, which is located at 1744 cm^{-1}, to the multicomponent band, quantifying its relative area after Fourier deconvolution. The fit of the component bands was done using the GRAMS 3.2 program (Galactic Inc.).

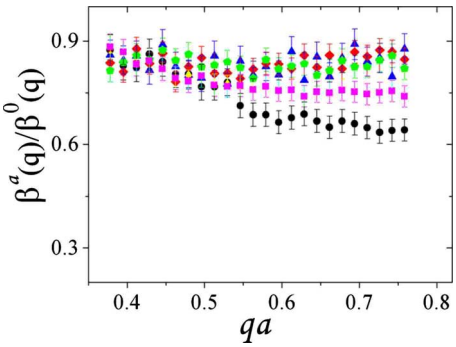

FIG. 2. (Color online) Experimental ratio $\beta^a(q)/\beta^0(q)$ from expression (18). [$MgCl_2$]: 5 (black circles), 7.5 (magenta squares), 10 (blue triangles), 30 (red diamonds), and 100 mM (green pentagons). This figure was shown in Ref. [10].

IV. RESULTS AND DISCUSSION

A. Effect of MIS and polydispersity

To understand the cluster morphologies, a precise and undoubted determination of the α exponent must be achieved. To do that, the effects of the aggregate polydispersity and MIS on the measured scattering exponents must be evaluated.

In relation to the MIS, the *normalized cross-correlation functions* $g_{12}^{\text{system}}(q,\tau)$ were measured and the ratio $\beta^a(q)/\beta^0(q)$ was calculated using expression (18) for all the examined electrolyte-liposome samples. In Fig. 2, the q dependence of $\beta^a(q)/\beta^0(q)$ is plotted for several samples. A remarkable q dependence of $\beta^a(q)/\beta^0(q)$ was observed for 5 mM (and a slight dependence for 7.5 mM). The rest of the samples exhibited a constant $\beta^a(q)/\beta^0(q)$ quotient over the explored q range. In these cases, therefore, the MIS has a constant contribution, which means that the values of the scattering exponents are not significantly affected by MIS. On the contrary, the 5 mM sample is very influenced by MIS. This is illustrated in Fig. 3, in which the effective structure factors determined with and without the MIS correction are plotted for this sample. As can be seen, if this correction is not performed we would obtain $\alpha^{\text{spurious}}(5\ \text{m}M)=3.12$ instead of 3.46 (the true value). This wrong result was also

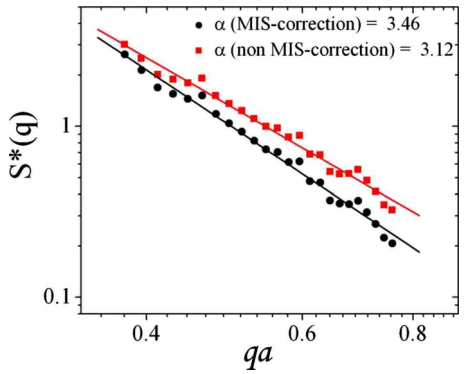

FIG. 3. (Color online) Experimental $S^*(q)$ at 5 mM of magnesium. Black circles correspond to expression (19) whereas red squares do not consider the MIS correction accounted for by $\beta^a(q)/\beta^0(q)$. Black and red solid lines stand for the corresponding linear fits.

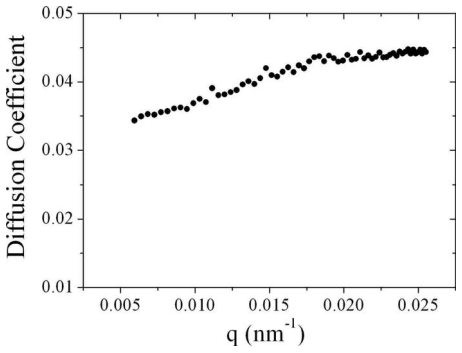

FIG. 4. Normalized mean translational diffusion coefficient $\bar{D}_{\text{expt}}(q;t)/D_0$ corresponding to the 100 mM magnesium concentration. A weak q dependence is revealed by the relative increment of $|\bar{D}_{\text{expt}}(q_{\max};t)-\bar{D}_{\text{expt}}(q_{\min};t)|/\bar{D}_{\text{expt}}(q_{\min};t)\approx 0.3$. D_0 is the free diffusion coefficient of the individual monomers.

confirmed within the experimental uncertainty by a conventional light scattering device with a single He-Ne laser beam (Malvern 4700IIC). Consequently, the use of a cross-correlation scheme based on three-dimensional light scattering design provides, under our experimental conditions, the necessary accuracy to discern the differences between dense clusters.

On the other hand, the polydispersity reached in an aggregation process can introduce a drastic disturbance on the scattering exponents determined by means of SLS when the cluster size distribution is broad. In these situations, a direct interpretation of the scattering exponents as fractal dimensions can cause misunderstandings. According to the work by Martin *et al.* [37], we have examined the experimental q dependence of the first cumulant of the field autocorrelation function divided by q^2, κ_1/q^2, for all the stopped suspensions [expressions (11) and (12)]. As was previously discussed, this ratio can be interpreted as an apparent mean translational diffusion coefficient $\bar{D}_{\text{expt}}(q;t)\equiv\kappa_1/q^2$ of the cluster distribution. It should be clear that in this context we explore the q dependence of κ_1/q^2 for nonevolving suspensions at a time at which the aggregates of these suspensions have achieved their final fractal structure and the aggregation processes have been stopped (see Sec. III C). In this framework, $\bar{D}_{\text{expt}}(q;t)$ will present a clear dependence on q, for $qR>1$, in the case of a wide cluster polydispersity (here R stands for the apparent mean hydrodynamic cluster radius). In our experiments, the evaluation of $\bar{D}_{\text{expt}}(q;t)$ over the q range $[6\times10^{-3},2.6\times10^{-2}]$ nm^{-1} showed a weak q dependence for all the examined samples. The maximum increment detected for $\bar{D}_{\text{expt}}(q;t)$ was approximately 30% corresponding to the 100 mM sample (see Fig. 4). This result is consistent with those obtained for aggregation kinetics, as we will argue later, being evidence for a narrow cluster distribution, and consequently a weak regime of polydispersity.

B. Discussion of the structure factors and cryo-TEM images

According to the previous protocol, the experimental $S^*(q)$ were determined for all the electrolyte concentrations and an unquestionable power law dependence was obtained in each case (see Fig. 5), from which the scattering exponents α were extracted. Table I also summarizes the results for the considered electrolyte-liposome samples. The absolute error associated with each exponent was estimated from the statistical reproducibility of the scattering data by their optimum power law fit. From this analysis, a clear trend is revealed: α decreases with increasing magnesium concentration, reaching a permanent value in the vicinity of 30 mM. The α values in the range 2.6–2.9 are a sign of dense morphologies that can be clearly identified as mass fractal with $d_m=\alpha$ [expression (5)]. On the other hand, after a careful analysis of the experimental data (which includes the MIS and polydispersity effects), structure factors with $\alpha>3$ reveal the existence of surface fractals [see again expression (5)]. Consequently, within the range $5\leqslant[\text{MgCl}_2]\leqslant15$ mM, the resulting morphologies, included in the domain of surface fractals, will present a surface fractal dimension $d_s=6-\alpha$. The surface fractal domain has Porod's law, $d_s=2$, as the lowest limit for a smooth surface [21], whereas $d_s\to3$ corresponds to the highest limit for a completely rough surface. Our surface fractal dimensions are contained within $d_s(5\text{ m}M)=2.54\pm0.08$ and $d_s(15\text{ m}M)=2.96\pm0.05$.

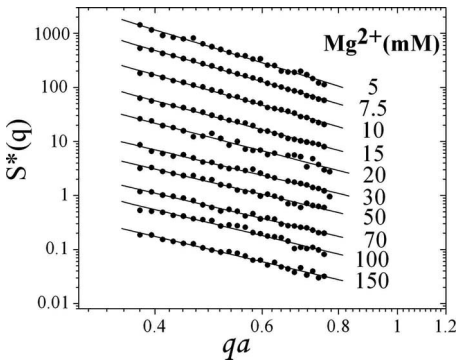

FIG. 5. Effective structure factors $S^*(q)$ for the different magnesium concentrations. The experimental values (circles) result from expression (19) whereas solid lines represent the theoretical fit according to expression (5). The content of this figure was shown in Ref. [10].

TABLE I. Experimental scattering exponents α with their corresponding fractal dimensions at different magnesium concentrations.

$[Mg^{2+}]$ (mM)	α	d
5	3.46 ± 0.08	$d_s = 2.54 \pm 0.08$ $(d_m = 3)$
7.5	3.28 ± 0.05	$d_s = 2.72 \pm 0.05$ $(d_m = 3)$
10	3.18 ± 0.05	$d_s = 2.82 \pm 0.05$ $(d_m = 3)$
15	3.04 ± 0.05	$d_s = 2.96 \pm 0.05$ $(d_m = 3)$
20	2.91 ± 0.12	$d_m = 2.91 \pm 0.12$
30	2.68 ± 0.07	$d_m = 2.68 \pm 0.07$
50	2.67 ± 0.08	$d_m = 2.67 \pm 0.08$
70	2.66 ± 0.06	$d_m = 2.66 \pm 0.06$
100	2.65 ± 0.07	$d_m = 2.65 \pm 0.07$
150	2.67 ± 0.08	$d_m = 2.67 \pm 0.08$

Certainly, the above interpretation of the experimental $S^*(q)$, obtained from expression (19), is based on the conservation of the form factor $P(q)$ of the primary particles inside the aggregates [see the cancellation between expressions (6) and (7) to give expression (8)]. In this respect, it is essential to prove that we extract the real structural information from the scattered intensity when we deal with aggregates formed by primary particles that are deformable and potentially fusionable. Thus, it is frequent to find in the literature dramatic distortions due to the deformation of the vesicles when they stick together [45,46]. In these situations, the vesicles lose their original shape, and $P(q)$ included in expression (6) is no longer their form factor after aggregation. Then, the implicit cancellation assumed in expression (8) is not admissible and the resulting q dependence is not only due to $S(q)$. However, this misinterpretation of $S(q)$ due to the deformation of the primary particles will be manifested only at large q values ($q \geqslant a^{-1}$). This is the range for which the details of the shape of the vesicles can be clearly distinguished via SLS. In this respect, our measurements of $S^*(q)$ were performed for $qa < 0.8$. Therefore, only for large values of this q region would the plausible disturbance introduced by the deformation of the particles have some effect on the determination of $S^*(q)$ via expression (19). Thus, one would expect poorly correlated results, presumably far from a power law behavior, only at large q if the vesicles change their shape when they aggregate. However, in our case, the same experimental power law behavior is manifested within the whole q range (see Fig. 5) and, therefore, a nonsignificant deformation of the vesicles inside the aggregates can be presumed. This experimental fact can be use as argument to discard not only an important deformation but also other severe distortions such as vesicle fusion, for which the primary particles would not retain their individuality.

From a theoretical viewpoint, the small deformation of our vesicles assumed from the experimental behavior of $S^*(q)$ at large q can be accounted for by the approach proposed by Petsev [47]. In his paper, the author presents a general model for vesicle adhesion based on the coupling between van der Waals attraction and bending elasticity forces. Using standard values for Hamaker's constants, this author shows calculations that are relevant for vesicles in which the ratio between the bilayer thickness and the vesicle radius is around 0.01. Together with this ratio, a significant deformation is expected only when the ratio between the separation distance of two adhered vesicles and the vesicle radius is smaller than 0.02. In our case the first ratio is much greater, 0.06. Although no experimental data are available for the separation distance between two adhered PS vesicles in the presence of magnesium, works like that cited in Ref. [39] by Ohki and Arnold, suggest a ratio between the separation distance and the particle radius of about 0.02–0.03. Accordingly, in the light of this model, a small deformation, consistent with our experimental data, is expected for our vesicles.

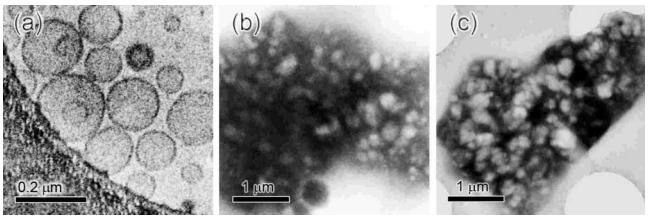

FIG. 6. Cryo-TEM images of PS liposomes in water (a) and after 5 min in water containing 7 mM of $MgCl_2$ (b), (c). Dark areas indicate the presence of crystalline ice (amorphous ice appears as transparent area in images).

In addition to the experimental $S^*(q)$, we took cryo-TEM images of different samples. Figures 6(b) and 6(c) show micrographs corresponding to two aggregates at 7 mM of $MgCl_2$. Uniform clusters can be observed in both cases. Thus, this high compactness would support and illustrate the interpretation that the high values obtained for the α exponent in these cases (5 and 7.5 mM) are associated with a surface fractal structure.

Accordingly, we can state that a transition from surface fractals to mass fractals has been found in the range from 5 to 150 mM of magnesium. The reader should note, however, that this interpretation cannot be made if the experimental data are not MIS corrected, particularly at low salt concentrations (<10 mM). As discussed previously, in the case of uniform clusters, the MIS effect is stronger at high q values, i.e., small spatial scales, as the experimental function $\beta^a(q)/\beta^0(q)$ reveals (Fig. 2). At these scales, the light experiences more reflections in uniform clusters than in those which are less compact and thus the MIS has an effect on the measured fractal dimensions.

Certainly, very few structures of biological interest have been described using the surface fractal notion [42]. On the other hand, similar morphological evolutions have been rarely documented in colloidal physics using small-angle scattering techniques. For instance, the pioneering results obtained by Keefer and Schaefer [8] in a system of rough particles made from silica condensation show a clear analogy with our measured fractal dimensions, even though they studied a significantly different system. In that work, the authors pointed out the application of the Eden model [41] to account for a theoretical description of the observed fractal structures. In any case, we should remark that our observed dilation symmetries need deeper investigation to be theoretically justified.

C. Qualitative interpretation of morphologies using hydration energies

We have concluded from the previous data that, when the Mg^{2+} concentration increases from 5 to 150 mM, the corresponding clusters experience a transition from uniform ($d_m=3$) to structures that are also dense, $d_m=2.6-2.7$. In the framework of a classical DLVO qualitative analysis, this high compactification would be explained by means of an aggregation in a secondary shallow minimum of the total interaction energy $E=E_{\mathrm{elec}}+E_{\mathrm{vdW}}$, whose depth is electrolyte dependent since the increase of a divalent salt leads to a progressive screening of the surface charge. However, some difficulties arise when a comparison with the aggregation induced by calcium is made [9]. Aggregation induced by $CaCl_2$ showed a slow regime (reaction-limited cluster aggregation) from 2.5 to 5 mM calcium concentration, and a DLCA regime from 5 to 7 mM was documented. In both cases, *ramified* structures were observed ranging from $d_m=1.91$ to 1.75. In this situation, the energy of the bond between two liposomes after sticking (accounted for by the van der Waals attraction) prevents reversibility and cluster compactification. Thus, as an example, whereas 5 mM of magnesium leads to a *dense* morphology, $d_m=3$, an identical calcium concentration induces branched structures, $d_m=1.75$. This experimental behavior suggests that the bound between two vesicles would be appreciably stronger in the case of calcium. In any case, the DLVO picture, $E=E_{\mathrm{elec}}+E_{\mathrm{vdW}}$, cannot explain why the behaviors in the presence of calcium and magnesium at identical concentrations are so different since both are divalent cations. Hence, we turn our attention to the possible specific effect of the hydration energy in the presence of these two cations via the determination of the hydration grade of the liposome surfaces. The Fourier-transform infrared spectroscopy analysis provides us this possibility. As a result of this analysis, Fig. 7 shows the component bands of the fine structure of the deconvolved spectra of PS liposomes in the carbonyl stretching zone (black) in D_2O at 0, 2.5, 5, and 7 mM of $CaCl_2$. In D_2O, the stretching CO band is composed of three bands located at 1744 cm^{-1} (green), 1727 cm^{-1} (yellow), and 1708 cm^{-1} (blue). These bands are a consequence of the different hydration grades of the CO groups of the two hydrocarbon chains. Thus, each one of the component bands is exclusively the result of the hydration state of the two CO groups of the phospholipid and, if no isotopic labeling of the carbonyl group is performed, no differences between them can be observed [43]. As a result, the previously noted component bands observed in D_2O originate from the dehydrated carbonyl (1744 cm^{-1}), the monohydrated carbonyl (1727 cm^{-1}), and the dihydrated carbonyl (1708 cm^{-1}). As can be observed, there is a progressive increment of the relative area of the 1744 cm^{-1} band (green)—corresponding to dehydrated CO—as Ca^{2+} concentration increases. At the same time, at $CaCl_2$ concentrations of 2.5, 5, and 7 mM the experimental stretching band is composed of five component bands. These two supplementary bands are located in the low-wave-number zone of the experimental carbonyl band. This fact indicates that, in the presence of the salt, the CO groups undergo a new type of interaction not present in pure D_2O. At high Ca^{2+} concentrations these changes have been explained by different rotational chain isomers in the lipid-Ca^{2+} complex and a new strong hydrogen bond established between CO and water [43]. Our results show that the effect of $CaCl_2$ on CO groups, as observed in the FTIR spectra, is concentration dependent and can be quantified. The relative areas of the deconvolved component bands showed that, when $CaCl_2$ was added to the aqueous medium, there was an increase of the area of the nonhydrated carbonyl band, which had no significant shift of its maximum at any salt concentration assayed. Thus, the microenvironment of the dehydrated CO is not affected by the presence of the divalent cation. At 2.5 mM of $CaCl_2$ this band had an area 16% larger than that in pure water, reaching a plateau at 5 mM, with a mean relative increment of 62%. Consequently, no further change occurs between 5 and 7 mM of $CaCl_2$ (filled green peak, Fig. 7). On the other hand, equivalent essays were performed in the presence of $MgCl_2$ over the range 0–20 mM. In that case, this carbonyl peak showed no significant change of the percentage area of its dehydrated carbonyl band in the range studied. Nevertheless, other functional groups of the phospholipid molecule, such as phosphate or carboxylate, should be explored in a further investigation in order to account for the evolution of the fractal dimension in the presence of this cation.

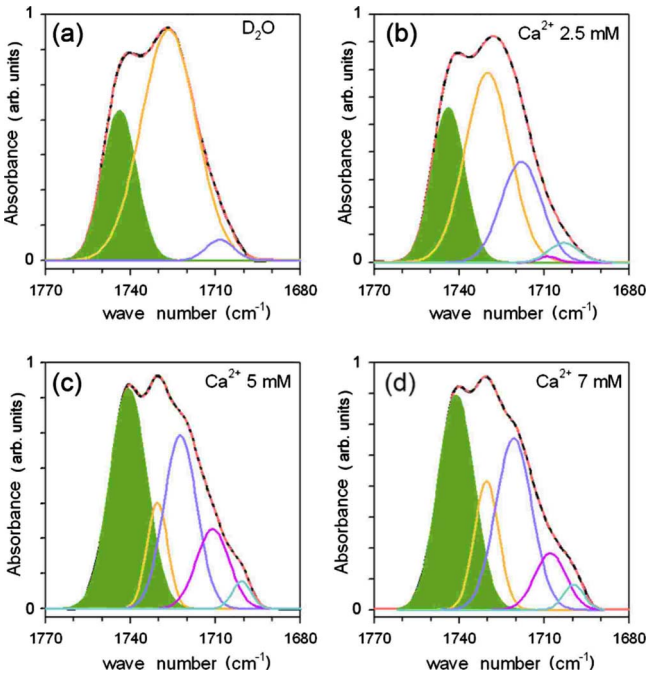

FIG. 7. (Color online) FTIR spectra of the carbonyl band of PS liposomes (a) in pure D_2O, [$CaCl_2$]=(b) 2.5, (c) 5, and (d) 7 mM. Black line: experimental deconvolved spectrum. Dashed light red line: synthetic spectrum obtained from the component bands (it overlaps the experimental band). Filled dark green peak: component band corresponding to the dehydrated carbonyl group. Other lines: component peaks corresponding to carbonyl groups with different hydration grades.

Consequently, we propose a qualitative analysis on the basis of the area of the nonhydrated carbonyl band. With calcium concentration, the increase in this area suggests a progressive dehydration of the liposome surfaces. Water

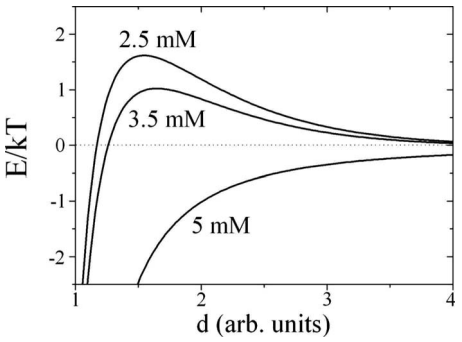

FIG. 8. Qualitative description of the interaction energy E at short distances between two liposomes in the presence of different calcium concentrations. With increasing calcium concentration the barrier resulting from the addition of hydration and Coulomb repulsive interactions decreases. At 5 mM, for which a DLCA regime was achieved [9], only a deep minimum due to van der Waals attraction remains. The distance d (arbitrary units) represents the separation between the membranes of the two liposomes.

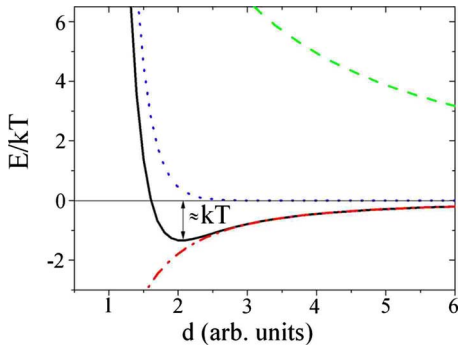

FIG. 9. (Color online) Qualitative description of the interaction energy E at short distances between two liposomes. The green dashed line stands for the repulsive Coulomb energy (according to a Yukawa functional form), the blue dotted line represents an exponentially decaying hydration energy [36], and the red dash-dotted line symbolizes van der Waals attraction. In simple terms, when magnesium is added, Coulomb repulsion is screened whereas the hydration interaction persists. The total energy in that case is therefore the result of the addition of van der Waals attraction and hydration repulsion (black solid line). This total energy presents a shallow minimum that conditions the dense cluster morphology of the magnesium induced aggregates. The distance d (arbitrary units) represents the separation between the membranes of the two liposomes.

molecules would be removed from the surface and the hydration repulsive interaction would become smaller. Consequently, the barrier due to this hydration energy would decrease and, if the Coulomb repulsion is strongly screened, the resulting total energy could therefore show a deep minimum essentially accounted for by the van der Waals attraction. For the sake of clarity we present in Fig. 8 a sketch with this qualitative interpretation. On the other hand, with magnesium, the dehydration of the lipid membrane associated with the carbonyl group would not take place and the hydration repulsive barrier would persist. Now the total interaction energy, when Coulomb repulsion is screened, $E \approx E_{\mathrm{vW}} + E_{\mathrm{hyd}}$ would present a "shallow" minimum with different depth depending on the magnesium concentration (see sketch in Fig. 9). Hence, this nonsuppressed hydration would condition the depth of the energy minimum as well as the separation distance for two bound vesicles. This lower energy minimum would enhance the cluster compactification.

These observations, involving calcium and magnesium, may be consistent with the model proposed by Ohki and Arnold [39], which is based on the addition of Coulomb and hydration repulsions together with van der Waals attraction. We should remark how these authors examine in this model a possible mechanism of ion-induced vesicle fusion. Furthermore, we would like to mention the analogy of our results with the recent work by Lu *et al.* [48] in which similar contrasting morphologies are documented, from confocal microscopy, in a suspension of colloidal spheres of polymethylmethacrylate. They obtain dense clusters, $d_m = 2.4-2.6$, which are induced by a "long-range" depletion attraction whereas they found ramified structures, $d_m = 1.7-1.8$, as a consequence of a "short-range" depletion attraction. In our opinion, the long-range depletion in this particular aggregation plays the same role as the total energy in the presence of magnesium, whereas the total energy in aggregation of liposomes induced by calcium is equivalent to their short-range depletion attraction.

D. Diffusion coefficient

Experimental data for the time evolution of $\bar{D}_{\mathrm{expt}}(q;t)$ obtained from DLS measurements according to the protocol presented previously are plotted in a double-logarithmic scale in Fig. 10. Figure 10(a) shows $\bar{D}_{\mathrm{expt}}(q;t)/D_0$ for the aggregation processes involving dense mass fractal aggregates (magnesium concentrations of 30, 100, and 150 mM), whereas the results corresponding to surface fractal populations (magnesium concentrations of 5 and 7 mM) are shown in Fig. 10(b). In both cases, all the experimental aggregation

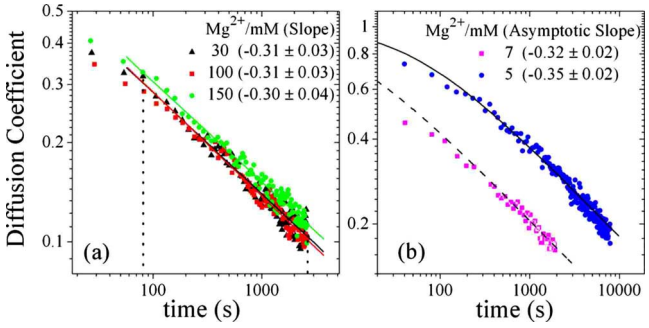

FIG. 10. (Color online) Normalized experimental mean diffusion coefficient $\bar{D}_{\mathrm{expt}}(q;t)/D_0$ as a function of time. (a) Mass fractals at different magnesium concentrations: 150 (green circles), 100 (red squares), and 30 mM (black triangles). Linear fit at long times are plotted as solid lines and their corresponding slopes appear in parentheses. Vertical dotted lines denote the interpolation range. (b) Surface fractals at different magnesium concentrations: 5 (blue circles) and 7 mM (magenta squares). Solid and dashed lines show the numerical solution for Smoluchowski's equation.

kinetics data exhibit a long-time behavior consistent with $\bar{D}_{\mathrm{expt}}(q;t) \propto t^{-1/3}$ within the experimental uncertainty, in spite of the time shift between them. Expression (16) indeed suggests elucidation of this common asymptotic behavior by a simple relationship: $3=(1-\lambda)d_m$. A certain advantage can be taken from our experimental determination of d_m, which showed a common value $d_m=3$ for the 5 and 7 mM samples. In this case (surface fractals), a value $\lambda=0$ corresponding to a diffusive aggregation regime seems to be a convenient selection. Accordingly, the interaction picture discussed before is coherent with that type of regime since aggregation happens due to the presence of a shallow minimum at short distances without any long-range interaction disturbing the diffusive motion of the clusters before sticking.

As pointed out previously, both D_n and $N_n(t)$ are required in order to account for these experimental data by means of expression (13). The frequency $N_n(t)$ is obtained by solving Smoluchowski's model under the assumption of a reaction kernel. As our SLS data indicate, we are dealing with uniform clusters. Due to their high compactness, these clusters can be considered as uniform objects, $d_m=3$, at least for surface fractal structures, whose size grows as $R_n \propto n^{1/3}$. This scaling growth together with our experimental determination $\lambda=0$ and the assumption of the Stokes-Einstein relation $R_n^{-1} \propto D_n \propto n^{-1/3}$ lead us to the *classical* Brownian kernel $k_{ij} \propto (R_i^{1/3}+R_j^{1/3})(D_i^{-1/3}+D_j^{-1/3}) \propto (i^{1/3}+j^{1/3})(i^{-1/3}+j^{-1/3})$ as a formal choice [37]. In this context, the small-large cluster reaction exponent, which also incorporates the collision cross section of the aggregates ($k_{1j} \propto j^{\nu}$, $j \to \infty$), is $\nu=1/3$. Therefore, the theoretical asymptotic behavior will be essentially conditioned by the cluster compactness, i.e., by d_m. Under this framework, the aggregation processes will be dominated by the small-large cluster reactions and thus cluster polydispersity will be discouraged [37]. This aspect is corroborated by the weak q dependence of $\bar{D}_{\mathrm{expt}}(q;t)$ (see Sec. IV A). As a conclusion, if we consider two diffusion-limited aggregation processes involving two different populations of surface fractals, i.e., populations with different d_s, the same values $\lambda=0$ and $\nu=1/3$ should be expected, independently of d_s.

In practice, it is found that a constant kernel ($k_{ij}=k_{11} \forall i,j$) reproduces essentially the same solution as the *classical* Brownian kernel even at moderately long times. Thus, the experimental values of the diffusion coefficient for the aggregation processes involving surface fractals were fitted using k_{11} as the unique free parameter. Figure 10(b) shows the results of these fits: in both cases the agreement is good even at short times. The delay between these two aggregation processes is theoretically accounted for by $k_{11}(5\ \mathrm{m}M)=(2.5\pm0.5)\times10^{-19}\ \mathrm{m}^3\ \mathrm{s}^{-1}$ and $k_{11}(7\ \mathrm{m}M)=(1.6\pm0.3)\times10^{-18}\ \mathrm{m}^3\ \mathrm{s}^{-1}$. In our opinion, this delay is due to the different strength of the bond between two vesicles at different magnesium concentrations. At 7 mM the roughness is higher than that at 5 mM and thus a vesicle will be, in general, surrounded by fewer neighbors on the surface of an aggregate, since the effective small-large captures are more likely during the aggregation process. Therefore, the different values of d_s have influence only on the delay time during the aggregation process but not on the asymptotic behavior as expected.

This discussion seems to be a key to understanding the aggregation kinetics results obtained for dense mass fractals [Fig. 10(a)] even though they need a more complex model to account for them completely. Nevertheless, the mass fractal dimensions obtained at 30, 100, and 150 mM magnesium concentrations are not far from that associated with a uniform object ($d_m=3$). In this respect, as we pointed out previously, the experimental values of $\bar{D}_{\mathrm{expt}}(q;t)$ show a similar long-time tendency to that corresponding to surface fractals. In addition, no structural differences were found within the range $30 \leqslant [MgCl_2] \leqslant 150$ mM (see Table I), i.e., the strength of the bond between two vesicles was not increased within this range. This is also supported by the aggregation kinetics data shown in Fig. 10(a), where identical kinetics results (without a delay time between them) are obtained at 30, 100, and 150 mM, which is evidence for a common kinetics within $30 \leqslant [MgCl_2] \leqslant 150$ mM.

In spite of the good qualitative, and even quantitative, description offered by our basic diffusive model, it should be stressed that other plausible options of reactive kernels could prove useful in order to account for the aggregation kinetics in the presence of magnesium. Certainly, our interpretation is based on the simplified interaction picture sketched in Fig. 9 together with the experimental evolution of $\bar{D}_{\mathrm{expt}}(q;t)$ and the measured fractal dimensions. This experimental phenomenology and the *a priori* interaction scenario lead us to a basic diffusive aggregation regime, $\lambda=0$, if we apply the van Dongen and Ernst scheme. Thus, the classical Smoluchowski Brownian kernel seems a sensible choice. However, the previous picture is not the unique possibility. In this respect, a reaction kernel with a sticking probability [49] obtained from the intervesicle interaction could be effective in order to explain the evolution of the measured mass fractal dimensions (from 3 to 2.6) upon increasing the magnesium concentration. This option was actually explored in our previous study in the presence of calcium [9], where the evolution from a slow to a DLCA regime was interpreted in terms of a decreasing repulsive barrier (see Fig. 8) and, consequently, an increasing sticking probability. In the present work, the evolution of the measured mass fractal dimensions when we increase the magnesium concentration is understood in terms of a small change in the depth of the energy minimum (Fig. 9), enhancing the strength of the bond between two adhered vesicles. This could be caused by a small reduction of the hydration repulsion as the magnesium concentration is increased. Nevertheless, a more exhaustive study of the fine structure of the IR absorption associated with the chemical groups of the phospholipid molecule is needed in order to elucidate this point. Furthermore, we feel that the use of the reaction kernel would be associated with additional fitting parameters governing the intervesicle interaction. Although the values of these fitting parameters would have a predictive meaning, they cannot be specifically contrasted with our current empirical phenomenology. Moreover, in our opinion, and due to the high compactification, a complete model should also contemplate reversibility through a Smoluchowski equation including fragmentation [50]. Undoubtedly, these refinements deserve to be contemplated in further studies although they are far from the scope of this work.

V. CONCLUSIONS

In this paper the aggregation processes of charged phosphatidilserine liposomes induced by the presence of magnesium have been studied. Static and dynamic light scattering, Fourier-transform infrared spectroscopy, and cryo transmission electron microscopy have been used as experimental techniques. The main conclusions are as follows.

(a) The structure of the liposome clusters shows a transition from uniform (surface fractals) to less dense structures (mass fractals) when the magnesium concentration increases. These morphologies contrast with those reported in the presence of calcium at similar electrolyte concentrations.

(b) We have proved that the multiple intracluster scattering has an influence on the determination of the fractal dimensions of the aggregates when they are very dense, i.e., at low magnesium concentration. In this respect, a careful experimental study of multiple intracluster scattering, based on a cross-correlation scheme, has been performed in order to obtain reliable values of the fractal dimensions. If this effect is not properly corrected for, fractal dimensions could be wrongly determined.

(c) We have shown that the classical DLVO model cannot explain the different morphologies documented in the presence of calcium and magnesium at identical concentrations. As a result, the hydration energy between liposomes due to the presence of magnesium and calcium should be introduced in order to explain (at least qualitatively) the different cluster morphologies. Thus, by means of Fourier-transform infrared spectroscopy, we propose measurement of the infrared absorption associated with the lipid head groups in order to provide a quantitative estimation of the hydration grade of the liposome surfaces.

(d) The kinetics of the aggregation processes has been studied through the time evolution of the mean translational diffusion coefficient of the aggregates. The experimental data were fitted solving Smoluchowski's equation. It has been shown that the relationship between structure and kinetics is consistent.

ACKNOWLEDGMENTS

The authors are grateful to "Ministerio de Educación y Ciencia e Innovación, Plan Nacional de Investigación, Desarrollo e Innovación Tecnológica ($I+D+i$)," Projects No. MAT2006-12918-C05-01, MAT2006-12918-C05-02, and MAT2006-12918-C05-05, the European Regional Development Fund (ERDF), and "Consejería de Innovación, Ciencia y Tecnología de la Junta de Andalucía" (Project No. P07-FQM-02496) for financial support.

[1] D. D. Lasic, *Handbook of Biological Physics* (Elsevier, London, 1995).
[2] Y. Barenholz, Curr. Opin. Colloid Interface Sci. **6**, 66 (2001).
[3] B. B. Mandelbrot, *Fractals, Form, Chance and Dimension* (Freeman, San Francisco, 1977).
[4] D. A. Weitz, J. S. Huang, M. Y. Lin, and J. Sung, Phys. Rev. Lett. **54**, 1416 (1985).
[5] J. L. Carrillo, F. Donado, and M. E. Mendoza, Phys. Rev. E **68**, 061509 (2003).
[6] L. Shen *et al.*, Langmuir **17**, 288 (2001).
[7] P. Pfeifer and J. Avnir, J. Chem. Phys. **79**, 3558 (1983).
[8] K. D. Keefer and D. W. Schaefer, Phys. Rev. Lett. **56**, 2376 (1986).
[9] S. Roldán-Vargas, A. Martin-Molina, M. Quesada-Perez, R. Barnadas-Rodriguez, J. Esterlrich, and J. Callejas-Fernández, Phys. Rev. E **75**, 021912 (2007).
[10] S. Roldán-Vargas, R. Barnadas-Rodríguez, A. Martín-Molina, M. Quesada-Pérez, J. Estelrich, and J. Callejas-Fernández, Phys. Rev. E **78**, 010902(R) (2008).
[11] B. V. Derjaguin and L. Landau, Acta Physicochim. URSS **14**, 633 (1941).
[12] E. J. V. Verwey and J. T. D. Overbeek, *Theory of the Stability of Lyophobic Colloids* (Elsevier, Amsterdam, 1948).
[13] S. Marcella, Chem. Phys. Lett. **42**, 129 (1976).
[14] D. N. Petsev and P. G. Vekilov, Phys. Rev. Lett. **84**, 1339 (2000).
[15] J. Israelachvili and H. Wennerstrom, Nature (London) **379**, 219 (1996).
[16] J. Martin and A. Hurd, J. Appl. Crystallogr. **20**, 61 (1987).
[17] P. Pfeifer and M. Obert, *The Fractal Approach to Heterogeneous Chemistry* (Wiley, Chichester, England, 1989).
[18] T. Vicsek, *Fractal Growth Phenomena* (World Scientific, Singapore, 1988).
[19] H. D. Bale and P. W. Schmidt, Phys. Rev. Lett. **53**, 596 (1984).
[20] D. W. Schaefer, J. E. Martin, P. Wiltzíus, and D. S. Cannell, Phys. Rev. Lett. **52**, 2371 (1984).
[21] C. M. Sorensen, Aerosol Sci. Technol. **35**, 648 (2001).
[22] B. J. Berne and R. Pecora, *Dynamic Light Scattering* (Wiley, New York, 1976).
[23] Z. Chen *et al.*, Phys. Rev. B **37**, 5232 (1988).
[24] M. Lattuada, H. Wu, and M. Morbidelli, Phys. Rev. E **64**, 061404 (2001).
[25] G. Phillies, J. Chem. Phys. **74**, 260 (1980).
[26] K. Schatzel, J. Mod. Opt. **38**, 1849 (1991).
[27] J. K. G. Dhont and C. G. de Kruif, J. Chem. Phys. **79**, 1658 (1983).
[28] A. Moussaïd and P. N. Pusey, Phys. Rev. E **60**, 5670 (1999).
[29] G. Odriozola *et al.*, J. Colloid Interface Sci. **240**, 90 (2001).
[30] S. J. Jung *et al.*, Powder Technol. **88**, 51 (1996).
[31] D. E. J. Koppel, J. Chem. Phys. **57**, 4814 (1972).
[32] M. Y. Lin, H. M. Lindsay, D. A. Weitz, R. C. Ball, R. Klein, and P. Meakin, Phys. Rev. A **41**, 2005 (1990).
[33] M. L. Broide, Ph.D. thesis. Massachusetts Institute of Technology, 1988.
[34] M. Z. Smoluchowski, Phys. Z. **17**, 557 (1916).
[35] M. Z Smoluchowski, Z. Phys. Chem. **92**, 129 (1917).
[36] P. G. J van Dongen and M. H. Ernst, Phys. Rev. A **32**, 670 (1985).
[37] J. E. Martin, J. P. Wilcoxon, D. Schaefer, and J. Odinek, Phys. Rev. A **41**, 4379 (1991).

[38] D. M. LeNeveu, P. Rand, and V. A. Parsegian, Nature (London) **259**, 601 (1976).
[39] S. Ohki and K. Arnold, Colloids Surf., B **18**, 83 (2000).
[40] C. Haro-Perez *et al.*, J. Chem. Phys. **119**, 628 (2003).
[41] R. Jullien and R. Botet, *Aggregation and Fractal Aggregates* (World Scientific, Singapore, 1987).
[42] J. Schüler *et al.*, Biophys. J. **77**, 1117 (1999).
[43] W. Hübner and A. Blume, Chem. Phys. Lipids **96**, 99 (1998).
[44] V. Buzón, E. Padrós, and J. Cladera, Biochemistry **44**, 13354 (2005).
[45] S. Huebner *et al.*, Biophys. J. **76**, 3158 (1999).
[46] F. Bordi *et al.*, Biophys. J. **91**, 1513 (2006).
[47] D. N. Petsev, Langmuir **15**, 1096 (1999).
[48] P. J. Lu, J. C. Conrad, H. M. Wyss, A. B. Schofield, and D. A. Weitz, Phys. Rev. Lett. **96**, 028306 (2006).
[49] A. Di Biasio, G. Bolle, C. Cametti, P. Codastefano, F. Sciortino, and P. Tartaglia, Phys. Rev. E **50**, 1649 (1994).
[50] F. Family, P. Meakin, and J. M. Deutch, Phys. Rev. Lett. **57**, 727 (1986).